ELSEVIER

Journal of Power Sources 66 (1997) 107–113

JOURNAL OF POWER SOURCES

Influence of alloying with bismuth on electrochemical behaviour of lead–calcium–tin grid alloys

S. Zhong [a], J. Wang [a], H.K. Liu [a], S.X. Dou [a], M. Skyllas-Kazacos [b]

[a] *Institute of Materials Technology and Manufacturing, University of Wollongong, Wollongong, NSW 2522, Australia*

[b] *School of Chemical Engineering and Industrial Chemistry, University of New South Wales, Sydney, NSW 2052, Australia*

Received 15 August 1996; accepted 21 October 1996

Abstract

The effect of bismuth, in the range 0.002 to 0.073 wt.%, on the electrochemical properties of lead–calcium–tin–aluminium alloy in sulfuric acid solutions at room temperature and 50 °C is investigated by potentiodynamic and a.c. impedance methods. Bismuth is added to a common grid alloy of lead–calcium–tin–aluminium, and the amount of bismuth in the alloys depends essentially on whether the alloying process is governed by equilibrium or kinetic processes. Potentiodynamic measurements provide a qualitative overview of the activating, passivating and transpassivating processes that correspond to $Pb \rightarrow PbSO_4$, $PbSO_4 \rightarrow PbO_2$ reactions, respectively. Addition of bismuth increases the passivating current density, i_{pass}, and modifies the conductivity of the passivating film on the electrode surface. An increased anodic attack is observed from cyclic voltammetric measurements and a more porous oxide layer is detected by scanning electron microscopy for various bismuth additions. The results show that the relationship between the extent of the anodic attack and bismuth content is not linear.

Keywords: Alloys; Lead; Calcium; Tin; Bismuth; Electrochemical behaviour

1. Introduction

The influence of bismuth on the performance of lead/acid batteries has long been an area of interest, although considerable conflict over its true effects is found in the literature. Many recent publications have suggested that the presence of a certain amount of bismuth can be beneficial rather than deleterious [1]. From Devitt and Myers' early report [2], batteries using lead–calcium–tin grids that contained 7 to 420 ppm bismuth showed no ill-effect due to bismuth, and battery cycle life tended to increase with increasing bismuth content. Kelly and Hampson [3,4] systematically explored the effect of bismuth on lead and lead–calcium alloys. The effect of the addition of bismuth (over the 0.084–0.281 wt.% Bi range) on alloy corrosion was investigated by the linear sweep voltammetric (LSV) method [5]. It was concluded that the addition of bismuth to the alloy resulted in an overall decrease in maximum peak current density values, $i_{p,max}$, for the potentiodynamic curves as the additive rendered the alloy less susceptible to anodic attack (low $i_{p,max}$ value). The alloy containing 0.15 wt.% Bi displayed the least susceptibility to anodic corrosion. These results are in contrast, however, with the earlier reports of Brynsteva et al. [6] and Gonzales et al. [7].

Rice [8] and Koop et al. [9] reported the effect of bismuth on pure lead by cyclic voltammetric studies. The former found that the values of E_p (current peak potential) are increased by the presence of bismuth. It was concluded that bismuth in the positive lead electrode inhibits the oxidation of lead sulfate to lead dioxide, increases the amount of oxygen evolved, prevents the formation of a more porous sulfate film on the surface of the electrode due to an enhancement of the nucleation of lead sulfate, leaches from the electrode and, possibly, is deposited on the negative electrode. Koop et al. [9] proposed that bismuth produces a dual influence on the corrosion of lead beneath the $PbSO_4$ film: (i) alteration of the morphology of the $PbSO_4$ crystal (bismuth causes the development of a more porous film that promotes an increased attack of the underlying substrate); (ii) modification of the grain structure of lead which determines the extent of corrosion under the $PbSO_4$ film. The influence of bismuth content on grain refinement and subsequent corrosion behaviour has also been reported by Papageorgiou and co-workers [10,11] in terms of cyclic voltammetric and weight-loss measurements. The results confirmed a non-linear relationship between the oxidation of lead sulfate to lead dioxide and the bismuth content.

More recently, Lam et al. [12] reported the effect of bismuth additions on the metallurgical and electrochemical

PII S0378-7753(96)02535-9

properties of Pb–1.5wt.%Sb alloys. They demonstrated that the corrosion rate of the grid decreased with increase in bismuth content and that bismuth, up to 0.09 wt.%, did not affect the self-discharge behaviour of batteries.

Analysis of the literature, reveals that most studies have been performed on lead–bismuth binary alloys or lead–antimony alloys, and that only little information relates to the influence of bismuth on lead–calcium–tin alloys that are commonly used as battery grids. In a previous paper [13], we reported the effect of bismuth on the mechanical properties of lead–calcium–tin–aluminium grid alloys. The aim of the present study is to determine the effect(s) of bismuth addition on the passivating and anodic attack behaviour of a common lead–calcium–tin–aluminium alloy, as well as on the microstructure of the corresponding states.

Historically, bismuth has been considered to be an undesirable element in lead/acid batteries. Bismuth can be removed from lead by the traditional Kroll–Betteron (KB) lead-refining process. The solubility relation near the freezing point of lead [14] is represented by

$$\log([Ca]^3[Bi]^2) = 12.46 - 11160/T \quad (1)$$

where T is in degrees Kelvin; [Ca] and [Bi] represent the wt.% Ca and the wt.% Bi in liquid lead. From thermodynamic considerations, the amount of bismuth is therefore tied up with calcium. In a normal Pb–Ca–Sn grid-casting process, the temperature of the molten lead is kept around 480 °C. This results in higher bismuth solubility in the molten alloy. Nevertheless, Bi_2Ca_3 compound could be precipitated on cooling, according to the di-bismuthizing equation: $3Ca + 2Bi = Ca_3Bi_2$ for which Moodie [15] has calculated an equilibrium constant at 330 °C

$$K = [Ca]^3[Bi]^2 = 8 \times 10^{-7} \quad (2)$$

The calcium and bismuth contents in the molten lead vary on cooling, however, according to Eq. (1). From thermodynamic considerations and manufacturing convenience, therefore, higher bismuth contents (> 0.08 wt.% Bi) are not considered in the present study.

2. Experimental

A nominal composition of the alloy, Pb–0.07wt.%Ca–0.6wt.%Sn–(0.01–0.02wt.%)Al, was chosen as the base alloy (0.002 wt.% Bi was detected in the alloy). Aluminium in the alloy is used to prevent calcium oxidation. Bismuth (Aldrich, 99.9%) was added to the molten alloy at about 360 °C. Sample alloy rods (diameter: 10 mm) were gravity-cast manually at the above temperature in a steel mould and cooled in air. All sample rods were stored over four weeks before experiments. The alloy compositions, analysed by inductively coupled plasma spectroscopy (ICP) are listed in Table 1. Working electrodes were prepared by machining the sample rods to a diameter of about 5 mm (then measured accurately to ±0.02 mm). A thick insulated copper wire was welded on one end of the alloy rod to make good electrical contact and to hold the electrode rigidly. The specimen was then mounted in epoxy resin (Araldite) in a plastic holder and the end polished to expose the working electrode surface.

Table 1
Alloy composition by ICP analysis (wt.%)

Electrode no.	Ca	Sn	Al	Bi
1*	0.071	0.383	0.016	0.002
2	0.068	0.379	0.013	0.045
3	0.064	0.374	0.010	0.059
4	0.064	0.362	0.016	0.073

*A normal grid alloy, all samples were prepared by this alloy.

Electrochemical measurement results can be strongly dependent upon the electrode surface preparation before immersion in the test solution. In order to obtain good reproducibility, therefore, the same surface treatment method was employed throughout the experiments. The mechanical grinding and polishing techniques were those as described previously [13]. A three-compartment electrolytic cell, separated by glass frits, was used in the experiments. The reference electrode was $Hg/Hg_2SO_4(K_2SO_4$ saturated solution system) that terminated in a Luggin capillary; all potentials are reported with respect to this electrode. The counter electrode was either a pure-lead sheet or a platinum wire. Electrolytes used in the experiments were 0.5 M and 1.28 sp. gr. H_2SO_4 solutions, prepared from 98 wt.% H_2SO_4 at 25 °C (Univar AR) with double-distilled water. The electrolyte was de-aerated with high purity nitrogen for 1 h before immersion of the test electrode in the solution.

Constant temperature was provided by a thermostatically controlled water bath (Julabo refrigerated, circulated mode F10-MH, Germany). Potentiodynamic anodic polarization and cyclic voltammetric measurements were performed by a scanning potentiostat (Model 362, EG&G Princeton Applied Research) that was connected via a MachLab/8 interface (Analog Digital Instruments, AD Instruments Pty) to a Macintosh computer supported by Chart v3.3 software. The anodic polarization measurements were perfomed under the reference of standard *ASTM G5-87*. The open-circuit specimen potentials, i.e., the corrosion potentials, were recorded after 55 min of immersion (E_{55}).

The cyclic-voltammetric measurements were performed after the working electrodes were 'anodically stabilized' at 1400 mV in the electrolyte (1.28 sp. gr. H_2SO_4 solution) for 14 h or 'initiated' by sweeping to a positive limit of 2000 mV in the first cycle. The impedance measurements of the working electrodes at different conditioning potentils were performed by an electrochemical impedance analyzer (Model 6310 EG&G Princeton Applied Research) with an IBM computer and MS398 software. The microstructures of the sample alloys and the morphology of oxide passivating films were examined with an optical microscope, Leica NMR, and a scanning electron microscope (SEM), Leica 440.

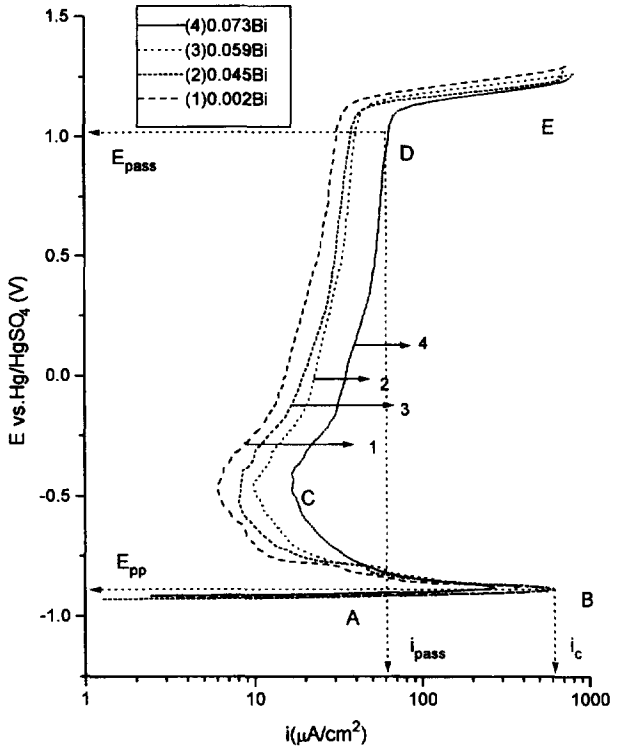

Fig. 1. Anodic polarization plots for different bismuth additions, sweep rate 0.2 mV s^{-1} at 20 °C in 0.5 M H_2SO_4.

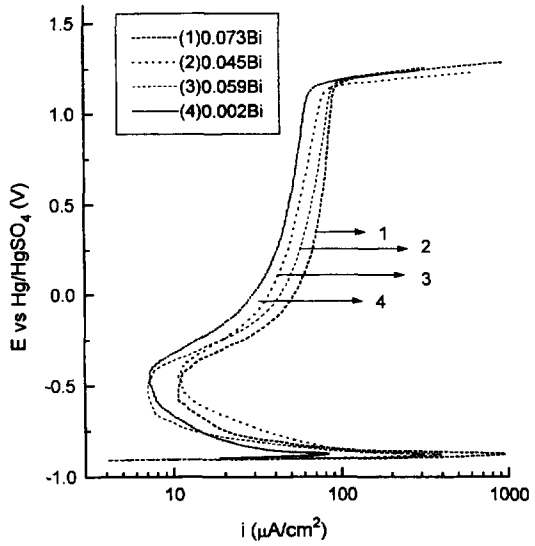

Fig. 2. Anodic polarization plots for different bismuth additions, sweep rate 0.2 mV s^{-1} at 50 °C in 0.5 M H_2SO_4.

3. Results and discussion

3.1. Potentiodynamic anodic polarization plots

Potentiodynamic anodic polarization plots at 20 and 50 °C in 0.5 M H_2SO_4 solution are presented in Figs. 1 and 2, respectively. Region A in Fig. 1 is the active region in which the specimen electrode corrodes as the applied potential is made more positive; this corresponds to the reaction: $Pb \rightarrow PbSO_4$. At point B, further increase in current density ceases and the onset of passivation commences. This point is characterized by two co-ordinate values, namely, the primary passive potential (E_{pp}) and the critical current density (i_c). In the region C, the current decreases rapidly as the passivating film forms on the specimen. A small secondary peak is observed after region C, where there is a change in current density as the potential is increased. With further increase in the applied potential, the passivating film begins to break down in region E, the transpassive region that corresponds to the reaction: $PbSO_4 \rightarrow PbO_2$. Data from these experiments at a given passive potential, E_{pass}, are presented in Table 2, where i_{pass} is the passive current density at the passive potential E_{pass}, and E_{55} is the corrosion potential at open circuit after 55 min of immersion. The passive layer has been demonstrated [17] to be a two-layer structure, i.e., $Pb/PbO_x/PbSO_4$. The instability of the passive layer, as evaluated by the passive current density, varies proportionally with the bismuth addition, but not linearly. The relationship between i_{pass} and bismuth content is plotted in Fig. 3. It is proposed that the bismuth additions could modify the two-layer structure and make the passive layer more conductive, i.e., the bismuth addition could have an effect on the passivation. This has been conformed by impedance measurements which are presented below.

3.2. Cyclic voltammetric measurements

Hampson and Kelly [3] reported that a 'stabilised electrode' could be obtained by cycling to a constant response between the limits 400 and 1520 mV in linear-sweep experiments. The stability of sample electrodes was evaluated by the maximum peak current values of the constant response curves, i.e., $i_{p,max}$ represents the anodic corrodibility.

In the present study, two electrode stabilization conditions were chosen. One condition was to raise the upper limit to 2000 mV in the first cycle, and then cycle between +500 to

Table 2
Data from potentiodynamic anodic polarization plots, Figs. 1 and 2

Electrode no.	20 °C			50 °C		
	E_{55} (mV)	i_{pass} (μA cm^{-2})	E_{pass} (V)	E_{55} (mV)	i_{pass} (μA cm^{-2})	E_{pass} (V)
1	−928	31.44	1.0	−913	60.40	1.0
2	−927	40.49	1.0	−910	83.11	1.0
3	−934	38.02	1.0	−918	73.45	1.0
4	−929	64.22	1.0	−915	87.52	1.0

+1600 mV, as described by Kellly and Hampson [5]. The rate of attainment of a constant response was studied by the following changes in peak current values (i_p) as the electrode was cycled. The percentage increase in peak current, ($i_p/i_{p,max} \times 100$), versus cycle number is plotted in Fig. 4. The other condition was to stabilize anodically the electrodes at +1400 mV for 14 h in the electrolyte before scanning. The results are given in Figs. 5–8. The peak current density values, i_p, for the PbO_2 formation peak attain a constant response after about 40 cycles. The peak current density values versus cycle number are given in Fig. 9 and provide information on the effect of bismuth on the oxidation of $PbSO_4$ to PbO_2. The results suggest that the bismuth additions can vary the kinetic barrier to the oxidation of $PbSO_4$ and accelerate the formation of PbO_2 from $PbSO_4$. The relation-

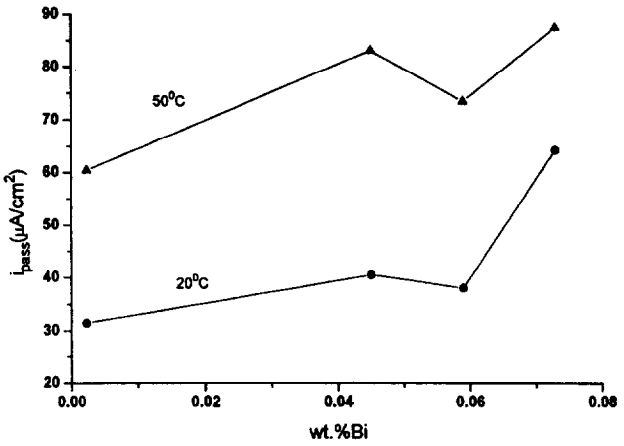

Fig. 3. i_{pass} vs. Bi content at E_{pass} = 1.0 V in 0.5 M H_2SO_4.

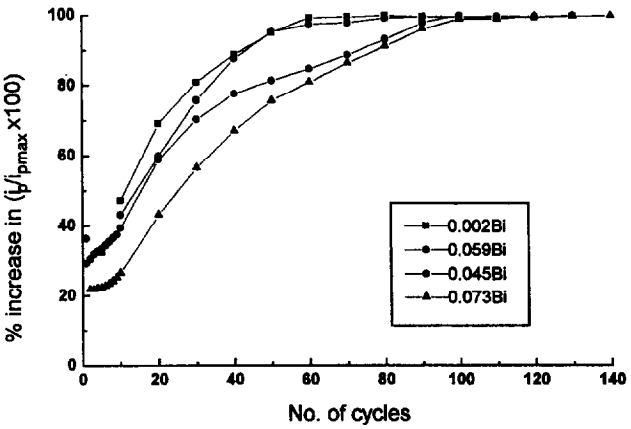

Fig. 4. Increase in peak current vs. cycle number with different bismuth contents, sweep rate 10 mV s^{-1} between 500 and 1600 mV in 1.28 sp. gr. H_2SO_4 at 20 °C.

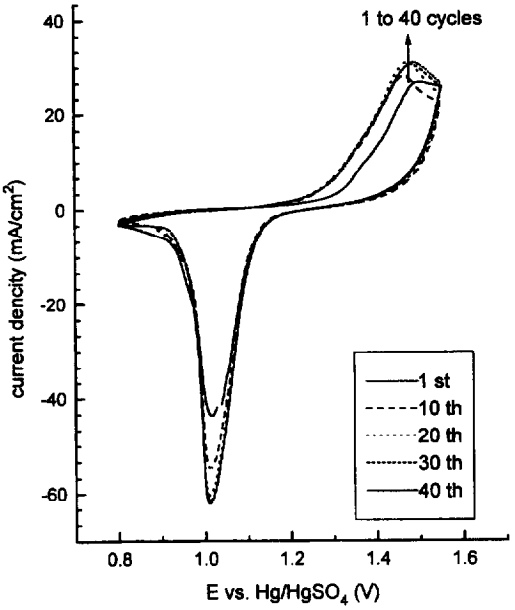

Fig. 6. Linear sweep voltammograms of 0.045 wt.% Bi electrode, held at +1.4 V for 14 h, sweep rate 10 mV s^{-1}, in 1.28 sp. gr. H_2SO_4.

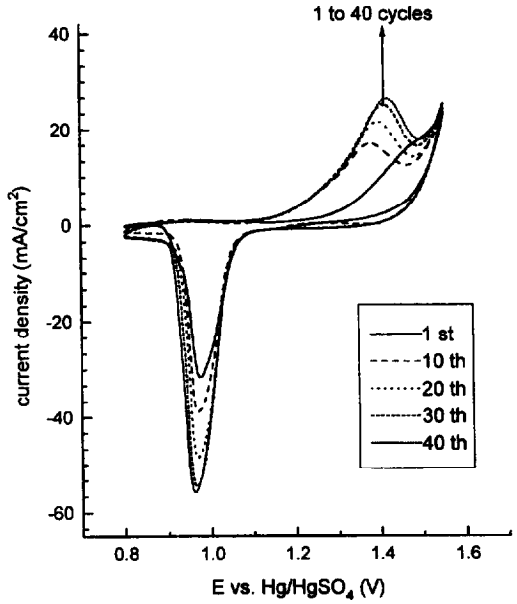

Fig. 5. Linear sweep voltammograms of 0.002 wt.% Bi electrode, held at +1.4 V for 14 h, sweep rate 10 mV s^{-1}, in 1.28 sp. gr. H_2SO_4.

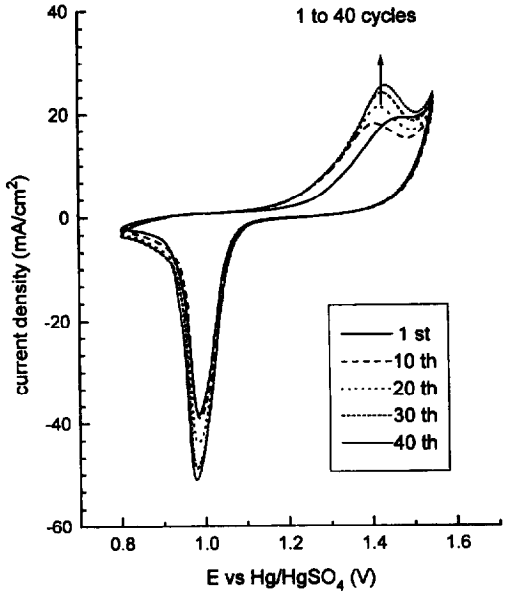

Fig. 7. Linear sweep voltammograms of 0.059 wt.% Bi electrode, held at +1.4 V for 14 h, sweep rate 10 mV s^{-1}, in 1.28 sp. gr. H_2SO_4.

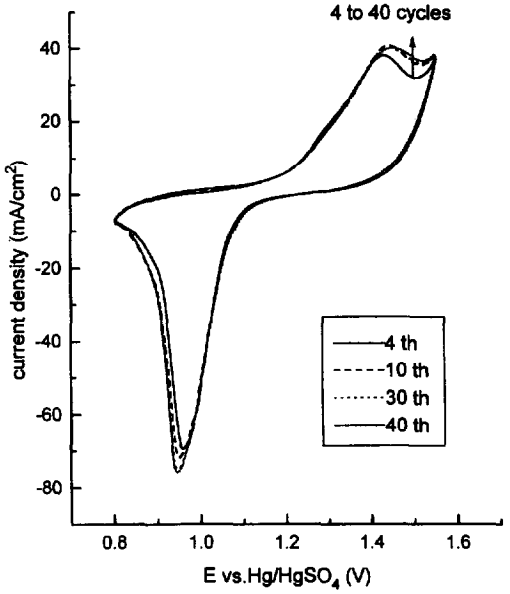

Fig. 8. Linear sweep voltammograms of 0.073 wt.% Bi electrode, held at +1.4 V for 14 h, sweep rate 10 mV s^{-1}, in 1.28 sp. gr. H_2SO_4.

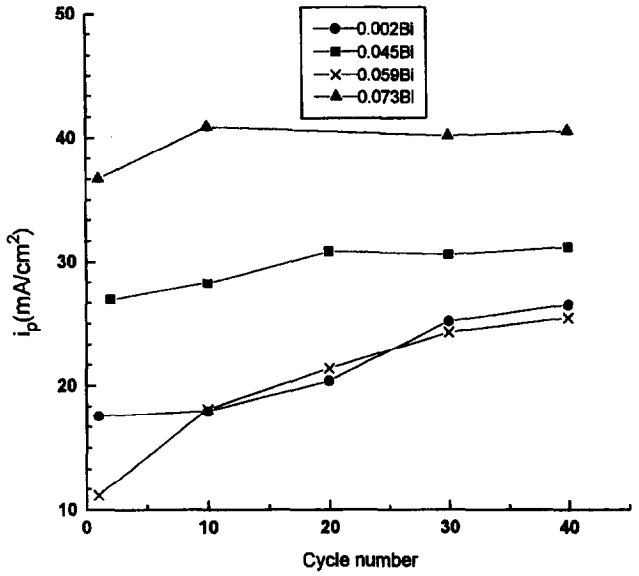

Fig. 9. Increase in peak current density values (i_p vs. cycle no. for different bismuth additions, data from cyclic voltammetry plots of Figs. 5–8.

ship between $i_{p,max}$ and bismuth concentration is plotted in Fig. 9, which shows a maximum anodic attack (high $i_{p,max}$ value) occurring at a bismuth content of 0.073 wt.%, but again the effect is not linear with the bismuth content. A possible explanation for this may due to the variation of the metallurgical microstructure of the alloys or/and of the morphology of the $PbSO_4$ crystals caused by the bismuth additions as described by Koop et al. [9]. The trend seen in Fig. 9, however, is consistent with that of Fig. 3.

3.3. Impedance measurements

Impedance measurements were performed in 0.5 M or 1.28 sp. gr. H_2SO_4 solutions at 20 °C in the range 100 kHz to 10 mHz at a conditioning potential of +900 mV, where a passive

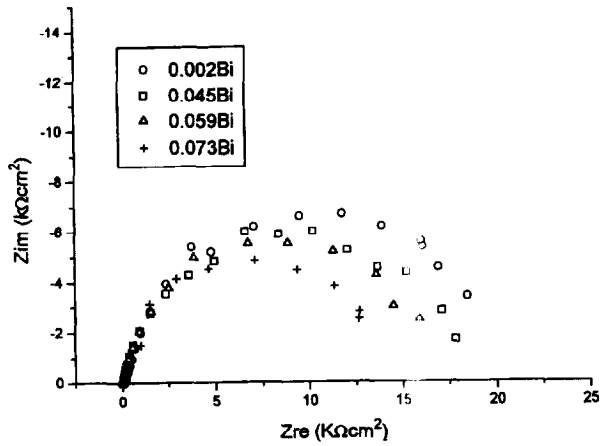

Fig. 10. Nyquist plots for (○) 0.002 wt.% Bi, (□) 0.045 wt.% Bi, (△) 0.059 wt.% Bi, and (+) 0.073 wt.% Bi in 0.5 M H_2SO_4 solution; conditional potential = +900 mV; conditional time = 3 h, and d.c. potential = +900 mV.

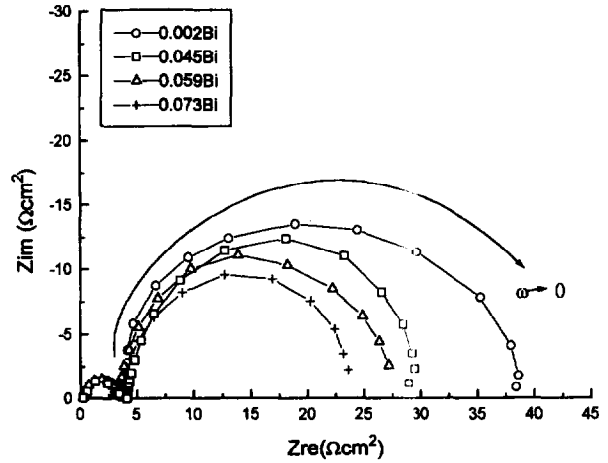

Fig. 11. Nyquist plots for (○) 0.002 wt.% Bi, (□) 0.045 wt.% Bi, (△) 0.059 wt.% Bi, and (+) 0.073 wt.% Bi in 0.5 M H_2SO_4 solution; conditional potential = +1500 mV; conditional time = 3 h, and d.c. potential = +1500 mV; ω is the frequency.

film is produced, and at a conditioning potential of +1500 mV where the passivating film breaks down and the PbO_2 layer appears. The test electrodes were held at the corresponding conditioning potential for 3 h before running the measurements. The results obtained are presented in the Nyquist plots shown in Figs. 10 and 11, respectively. According to the two-layer structure of the oxide film suggested by Pavlov and Iordanov [17], the inner oxide layer (PbO_x, $x = 1$–1.7) has a higher resistance than the outer one. The equivalent circuit proposed for lead alloys and a schematic diagram for the equivalent circuit are presented in Fig. 12(a) and (b), respectively. Impedance measurements thus show that an increase in the conductivity of the oxide passive films is observed with increase in the bismuth addition. This finding confirms the above results from the anodic polarization experiments.

3.4. Metallurgical and morphology examinations

The microstructure of the working electrode surface was examined by optical microscopy. The results are given in

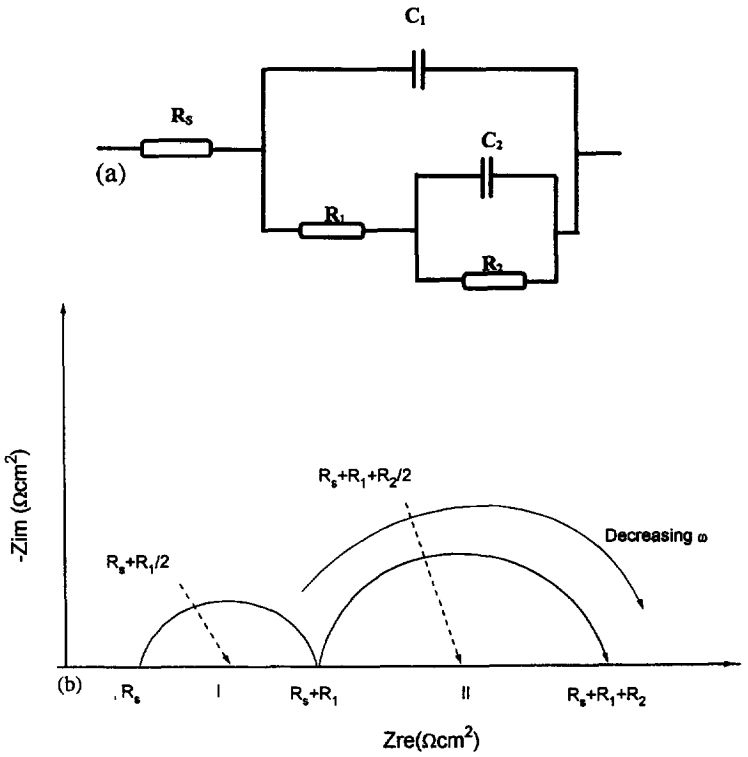

Fig. 12. (a) Proposed equivalent circuit for lead–calcium–tin–aluminium alloys with bismuth additions; R_s is the electrolyte resistance; R_1 and C_1 is the outer oxide layer resistance and the capacity ($PbSO_4$), respectively; R_2 and C_2 is the inner oxide layer resistance and the capacity (PbO_x) of the electrode surface, respectively. (b) Schematic complex-plane diagram for the equivalent circuit shown in Fig. 12(a).

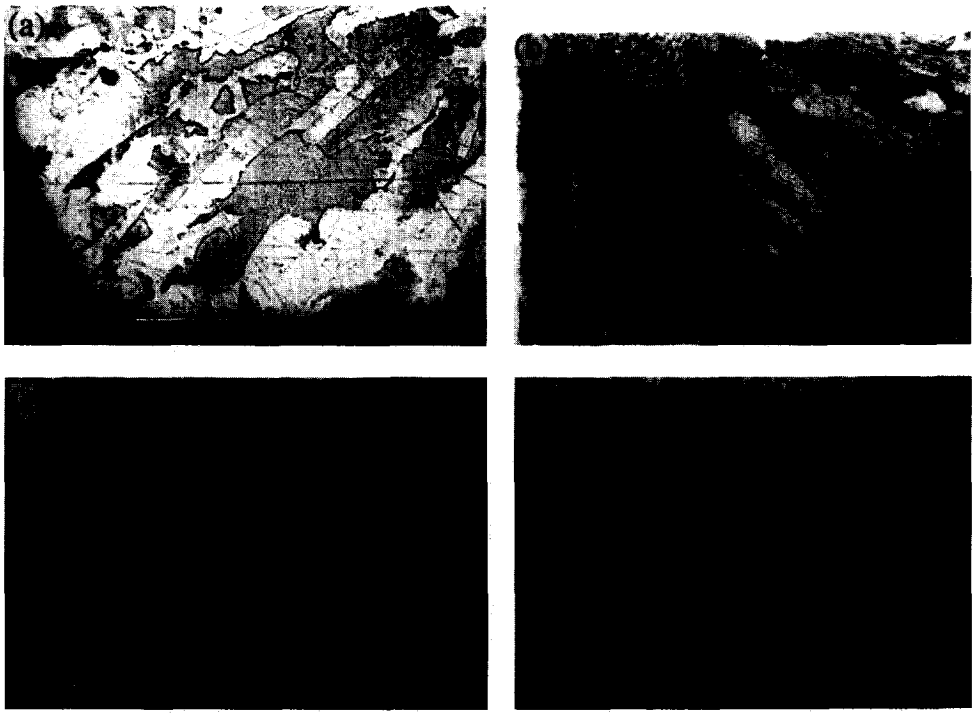

Fig. 13. Microstructure of Pb–Ca–Sn–Al grid alloys with different bismuth contents: (a) Bi = 0.002 wt.%; (b) Bi = 0.045 wt.%; (c) Bi = 0.059 wt.%, and (d) Bi = 0.073 wt.%.

Fig. 13. The metallurgical microstructure shows that the grain size and the grain form are also effected by the casting condition. This can been seen from the microstructure of the pure lead under this casting condition [18]. Several sample rods of each composition were cast and examination of different cross sections of each sample demonstrated that there is a good reproducibility of the microstructure analysis. The morphology of the $PbSO_4$ crystal and oxide passive films of the

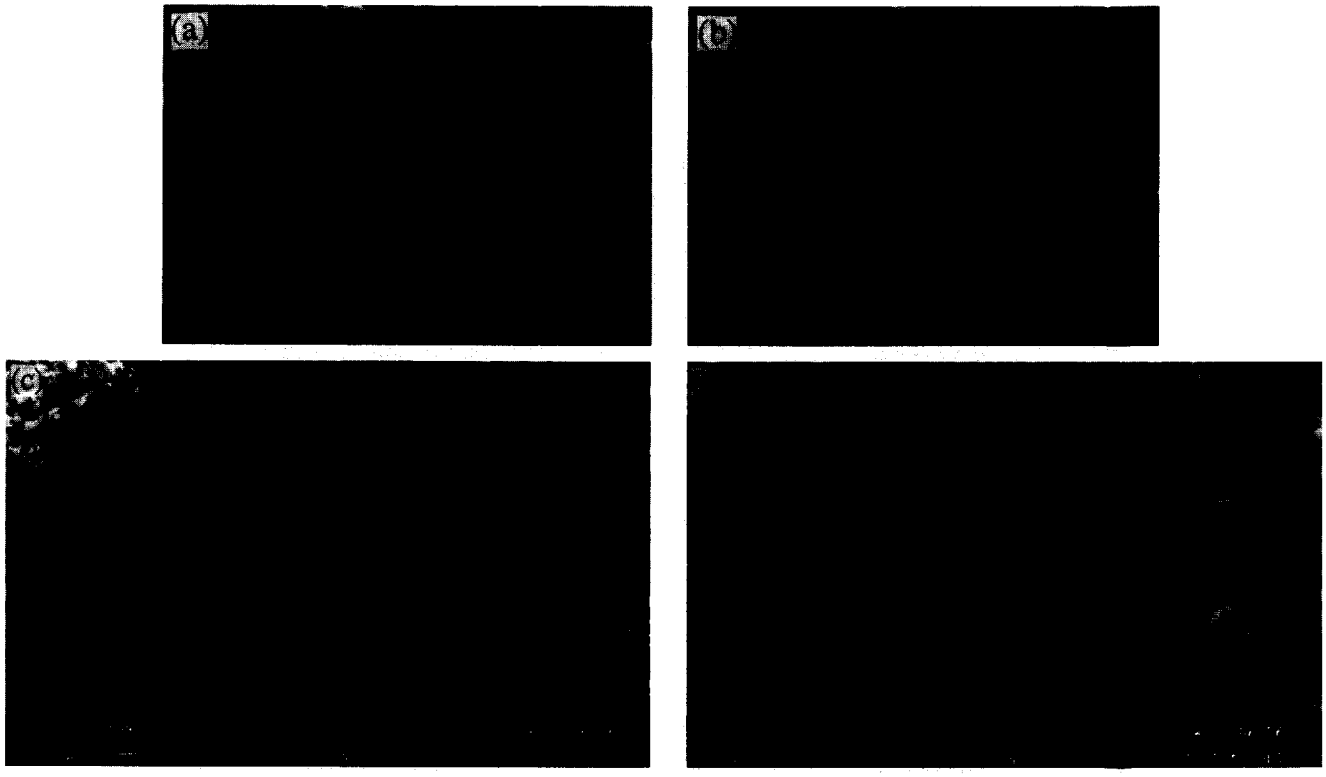

Fig. 14. (a)–(d) Morphology examinations of the oxide passivating films on working electrodes by SEM: (a) Bi = 0.002 wt.%, anodically polarized at +900 mV for 3 h in 1.28 sp. gr. H_2SO_4; (b) Bi = 0.045 wt.%, anodically polarized at +900 mV for 3 h in 1.28 sp. gr. H_2SO_4; (c) Bi = 0.002 wt.%, anodically polarized at + 1400 mV for 14 h in 1.28 sp. gr. H_2SO_4, and (d) Bi = 0.073 wt.%, anodically polarized at + 1400 mV for 14 h in 1.28 sp. gr. H_2SO_4.

working electrodes at a conditioning potential of 900 mV for 3 h was examined by SEM; the results are presented in Fig. 14(a) and (b). Similar examinations were performed on the electrodes in the transpassive state, i.e., at the conditioning potential of + 1400 mV for 14 h; the micrographs are shown in Fig. 14(c) and (d). It is found that the grain size is effected more by the casting condition than by the bismuth content. SEM results show that a more porous film appears with higher bismuth content. This again proves that bismuth promotes the development of a more porous oxide film and, in turn, increases the anodic attack of inner alloy substrate.

4. Conclusions

1. The incorporation of bismuth in lead–calcium–tin–aluminium alloys increases the passivating current density and improves the conductivity of the oxide passive film. This could produce a beneficial effect on the battery recharge performance and suppress 'passivation phenomena'.

2. An increased anodic attack is observed with the bismuth additions used in of this study. The effect is not linear.

3. Bismuth additions alter the morphology of the oxide and cause the development of a more conductive and porous film on the electrode surface.

References

[1] M.J. Koop, D.A.J. Rand and B. Culpin, *J. Power Sources, 45* (1993) 365.

[2] J.L. Devitt and M. Myers, *J. Electrochem. Soc., 123* (1976) 1796.

[3] N.A. Hampson and S. Kelly, *J. Electrochem. Soc., 127* (1980) 1456.

[4] N.A. Hampson and S. Kelly, *J. Appl. Electrochem., 11* (1981) 751.

[5] S. Kelly and N.A. Hampson, in J. Thompson (ed.), *Power Sources 8, Proc. 12th Int. Power Sources Symp., Brighton, UK, Sept. 1980,* Research and Development in Non-Mechanical Electrical Power Sources, Academic Press, London, 1981, p. 535.

[6] V.I. Bryntseva, V.G. Bundzhe, Y.D. Dunaev, G.Z. Kiryakov and L.A. Tskhe, *Zashch. Met., 3* (1967) 504.

[7] J.A. Gonzales, M. Rvêjula and S. Felui, *Rev. Met. (Madrid), 7* (1971) 105.

[8] D.M. Rice, *J. Power Sources, 28* (1986) 69.

[9] M.J. Koop, D.F.A. Koch and D.A.J. Rand, *J. Power Sources, 36* (1991) 369.

[10] N. Papageorgiou and M. Skyllas-Kazacos, *J. Power Sources, 36* (1991) 57.

[11] N. Papageorgiou, M. Skyllas-Kazacos and D.A.J. Rand, in T. Tran and M. Skyllas-Kazacos (eds.), *Proc. 7th Australian Electrochemical Conf. (7AEC), Sydney, Australia, 15–19 Feb. 1988,* Royal Australian Chemical Institute, 1988, pp. 32–35.

[12] L.T. Lam, T.D. Huynh, N.P. Haigh, J.D. Douglas, D.A.J. Rand, C.S. Lakshmi, P.A. Hollingsworth, J.B. See, J. Manders and D.M. Rice, *J. Power Sources, 53* (1995) 63.

[13] S. Zhong, H.K. Liu, S.X. Dou and M. Skyllas-Kazacos, *J. Power Sources, 59* (1996) 123.

[14] T.R.A. Devey, in J.M. Cigan, S. Mackey and T.J. O'Keefe (eds.), *Lead–Zinc–Tin '80,* American Institute of Mining Engineers, 1979, p. 477.

[15] J.M. Moodie, *M. App. Sci. Thesis,* University of Melbourne, 1976.

[17] D. Pavlov and N. Iordanov, *J. Electrochem. Soc., 117* (197) 1103.

[18] S. Zhong, H.K. Liu, S.X. Dou and M. Skyllas-Kazacos, *J. Power Sources,* submitted for pubication.